ACS APPLIED MATERIALS & INTERFACES

Research Article

www.acsami.org

Newly Observed Temperature and Surface Ligand Dependence of Electron Mobility in Indium Oxide Nanocrystals Solids

Hien Thu Pham and Hyun-Dam Jeong*

Department of Chemistry, Chonnam National University, Gwangju 500-757, Republic of Korea

Supporting Information

ABSTRACT: We developed a new class of organic surface ligands; 2-aminopyridine (2AP), 4-aminobenzoic acid (4ABA), and benzoic acid (BA); for use in the solution ligand exchange of nanocrystals (NCs) in the presence of nitric acid (HNO_3). Here, colloidal NCs synthesis is used for the first time. These short, air-stable, easy-to-model ligands bind to the surface of the indium oxide nanocrystal (In_2O_3 NC) and provide the electrostatic stabilization of NC semiconductor dispersions in *N*,*N*-dimethylformamide, allowing for a solution-based deposition of NCs into thin-film transitors (TFTs). The shorter organic ligands greatly facilitate electronic coupling between the NCs. For example, thin films made from 2AP-capped In_2O_3 NCs exhibited a high electron mobility of $\mu \approx 9.5$ $cm^2/(V{\cdot}s)$, an on−off current ratio of about $>10^7$, and a subthreshold swing of 2.34 V/decade. As the ligand length decreased, the electron mobility increased exponentially. Furthermore, we also report on the temperature-dependent behavior of the electron transport of In_2O_3 NCs films, in the case in which thin films were cured at 150 °C, as the 2AP, BA, and 4ABA ligand molecules were sustained on the NC. We demonstrated a hopping transport mechanism instead of a band-like transport, and the thermally activated carrier transport process governed the charge transport in our In_2O_3 NC thin-film solid.

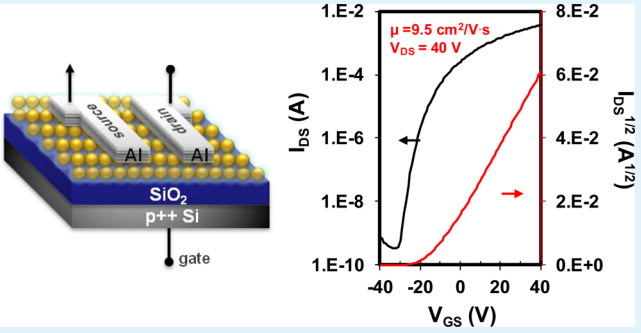

KEYWORDS: *In_2O_3 nanocrystals, ligand length dependence, temperature dependence, activation energy, thermally activated carrier transport*

INTRODUCTION

In recent years, the use of metal oxide semiconductors (MOSs) in electronics has been investigated, such as for field-effect transistors (FETs), due to their outstanding electrical properties, including a high carrier mobility and desirable optical transparency.[1] Indium oxide (In_2O_3) is an MOS that has been considered to be an important semiconductor, and it has a band gap of 3.6−3.75 eV at room temperature and an excellent single-crystal mobility of 160 $cm^2/(V{\cdot}s)$.[2,3] Despite the fact that the application of In_2O_3 into thin-film transistors (TFTs) through the use of a precursor[4−7] has been extensively investigated, the fabrication of In_2O_3 TFTs through a nanocrystal (NC) approach has not yet been achieved. Currently, various morphology-tuned In_2O_3 NCs have been extensively prepared and investigated by using fatty acids (e.g., myristic acid and oleic acid), fatty amines (e.g., trioctylamine and oleylamine), or their mixtures. Prominently, Park et al. first reported high crystalline and size-controlled In_2O_3 NCs from indium acetylacetone precursor ($In(acac)_3$) in the presence of oleylamine as stabilizing surfactants.[8] Morphological tuning and optical properties of In_2O_3 NCs were distinctly observed by Liu et al.[9] and Ye et al.[10] In continuing this investigation, our group recently described solution-processed oleic acid (OA)-capped In_2O_3 NC TFTs and found that the size of the NCs had an effect on the performance of the TFTs.[11] However, it has a number of drawbacks in that OA acted as a bulky insulating barrier between NCs, preventing charge transport, and the complete removal of the long hydrocarbon chain surface ligand by thermal treatment often generated multiple surface dangling bonds and midgap charge-trapping states and typically led to sintering of NCs.[12,13] Numerous literature reports studied the effect of the lengths of ligand molecules on charge transport in arrays of NCs, for instance PbS quantum dots, which shows that a strongly coupled, high mobility can be achieved by replacing bulky, insulating hydrocarbons that are used as ligands during synthesis with shorter ligands, which reduces the interparticle spacing and allows proximal NCs.[14−17] Here, we demonstrate the use of high-performance In_2O_3 NC TFTs with short molecules as ligands to reduce interparticle spacing and to improve mobility. We synthesized highly monodisperse In_2O_3 NC samples and replaced the long-chain organic ligand on the surface of the NCs by conducting a ligand exchange with a new class of organic ligands that includes 2-aminopyridine, benzoic acid, and 4-aminobenzoic acid. These are abundant, nontoxic, compact, and stable organic ligands that are capable of preserving the colloidal dispersibility of semiconductor NCs.

Received: April 7, 2015
Accepted: May 11, 2015
Published: May 11, 2015

DOI: 10.1021/acsami.5b02971
ACS Appl. Mater. Interfaces 2015, 7, 11660−11667

We used a single-step, low-temperature, solution-based process to form highly uniform and closely packed NC thin films. This approach enables wide-area NC thin films to be fabricated at a low cost. Here, we also describe how the electron mobility depends on the ligand length. Room-temperature measurement shows that the electron mobility increases exponentially as the ligand length decreases. The charge transport mechanism is elucidated by analyzing the temperature-dependent charge transport characteristics of the NCs in the temperature range 173 K < T < ~300 K by fabricating corresponding TFT devices. It is therefore important to understand the effect that the ligand has on the properties of the NC arrays to further exploit NC-based devices.

EXPERIMENTAL SECTION

Chemicals and Materials. Indium(III) acetate ($In(Ac)_3$, 99.99%), oleic acid (OA, ≥95%), 1-octadecene (ODE, 90%), *N*,*N*-dimethylformamide anhydrous (DMF, 99.8%), 2-aminopyridine (2AP, 99%), benzoic acid (BA, ≥99.5%), and 4-aminobenzoic acid (4ABA, ≥99%) were obtained from Sigma-Aldrich, 1-octadecanol (ODA, 97%) was obtained from Alfa Aesar, and all chemicals were used without further purification. Chloroform (≥99.5%), acetone (≥99.5%), methanol (≥99.5%), and nitric acid (HNO_3, 60%) were purchased from Daejung Chemicals (Siheung City, South Korea) and were used as received.

NC Synthesis. In_2O_3 Nanocrystals (In_2O_3 NC-OA). A 5.3 nm amount of oleic acid-capped In_2O_3 nanocrystals (In_2O_3 NC-OA) were synthesized following the procedure we had previously published.[11] In a typical reaction, precursor solution was introduced in a 50 mL three-neck flask and was loaded with 430 mg of In_2O_3, 1.28 g of OA, and 6.22 g of ODE. The solution was heated to 120 °C and was held under a vacuum for 2 h. A separate 250 mL three-neck flask containing ODA solution, including 12.72 g of ODA and 75 mL of ODE, was prepared, heated to 120 °C, and held under a vacuum for 2 h. After degassing both solutions in a vacuum at 120 °C for 2 h, the containers were refilled with Ar. The ODA solution was heated to 310 °C, and then the precursor solution was rapidly injected. The solution temperature was dropped to 294 °C and maintained for 13 min, and then the reaction was quenched. After the solution had cooled to 50 °C, the In_2O_3 NC-OA was collected via dissolution/precipitation using hexane and acetone solvents. The NCs were vacuum-dried for 12 h at 100 °C. A slightly yellow powder was collected and well-dissolved in various organic solvents.

Solution Ligand-Exchange Process. *2-Aminopyridine (2AP) and 4-Aminobenzoic acid (4ABA) in the Presence of Nitric Acid-Exchanged In_2O_3 Nanocrytals.* In a typical procedure 300 mg of as-synthesized NCs were dissolved in 30 mL of chloroform in a 40 mL vial. The ligand-exchange reaction was performed using a homogeneous mixture of chloroform and methanol as solvents. The ligand solution was prepared as follows. A 150 mg amount of ligand (2AP and 4ABA) in 3 mL of methanol was mixed with 150 mg of nitric acid. The ligand solution was added into the as-synthesized NC solution with vigorous stirring. The mixture solution had a pH of 2.0−2.2. When the target ligand solution was added, the NC solution became turbid. To accelerate the ligand-exchange reaction, the solution was heated to 60 °C, and then the NCs were allowed to precipitate to the bottom of the 40 mL vial over the next 5 h. The upper solution was decanted, and then, 10 mL of chloroform was added and stirred for 10 min. After the NCs had settled down, the upper solution was removed, and the NCs were washed one more time with chloroform. Then, 10 mL of methanol was added and stirred for 10 min, and the upper solution was removed via centrifugation at 15000 rpm for 5 min. Finally, 10 mL of chloroform was added and around 200 mg of the as-exchanged In_2O_3 NC was obtained in a powder form after drying with a rotary evaporator.

Benzoic acid (BA) in the Presence of Nitric Acid-Exchanged In_2O_3 Nanocrytals. The BA-capped NCs were prepared by developing a simple ligand-exchange procedure based on the phase transfer of NCs from a nonpolar organic medium (hexane) into a polar solvent such as DMF. Typically, 200 mg of the as-synthesized NCs was dissolved in 3.8 g of hexane in a 20 mL vial. A solution of 100 mg of BA in 5 mL of DMF was adjusted with 100 mg of nitric acid in another 20 mL vial. The ligand solution was added into the as-synthesized NC solution with vigorous stirring. To accelerate the ligand-exchange reaction, the solution was heated to 60 °C until the hexane phase turned colorless and a stable colloidal solution of NCs in DMF had formed. The upper hexane solution was decanted out, and then10 mL of toluene was added and stirred for 10 min. After the NCs had precipitated, the toluene solvent was removed via centrifugation at 15000 rpm for 2 min. Then, the NCs were dissolved once again in DFM. Then, this toluene/DMF washing process was repeated once more. Finally, 10 mL of toluene was added, and around 120 mg of the as-exchanged In_2O_3 NC was obtained in a powder form after drying using a rotary evaporator.

Fabrication of Thin-Film Transistors with Semiconductor Layers from In_2O_3 NC Produced by Ligand Exchange. In_2O_3 NC thin films were prepared by spin-coating a monodisperse, 3 wt % solution of the as-exchanged In_2O_3 NCs with 2AP, 4ABA, and BA ligands dispersed in DMF solvent on SiO_2/Si substrates at 3,000 rpm for 30 s. The substrates consisted of a 100 nm thick SiO_2 layer on a heavily doped p-type silicon wafer that served as the gate dielectric and gate, with a resistivity of <0.005 Ω·cm and a thickness of 525 ± 25 μm. The NC thin films were then cured at different temperatures (150 and 350 °C) for 3 h on a hot plate in an air atmosphere. Here, the Si-wafer substrates were precleaned to improve the wettability of the DMF coating solution on the surface of the Si wafer through a well-known piranha treatment. The Si wafer was immersed in a solution of H_2SO_4 (35 mL) and H_2O_2 (15 mL) at 110 °C for 6 h and was then fully washed with deionized water, ethanol, and acetone. Finally, the Al source/drain electrodes were thermally deposited on the NC layers by employing a shadow mask, which resulted in TFT devices with a channel length of 100 μm and a channel width of 1000 μm.

Characterization. Field-emission transmission electron microscopy (FE-TEM) was performed using a JEM-2100F electron microscope (JEOL, Japan) with an accelerating voltage of 200 kV. For the TEM sampling, 0.2 wt % solutions of as-synthesized NCs in toluene and as-exchanged NCs in DMF were drop-cast onto a carbon-coated copper grid, and the solvents were evaporated in a vacuum. Fourier transform infrared spectroscopy (FT-IR) was conducted on a Nicolet 380 spectrometer (Waltham, MA, USA). Thermal gravimetric analysis (TGA) was conducted using a METTLER TOLEDO SDTA851e. The samples were heated at a rate of 10 °C/min from room temperature to 800 °C in a dried-air atmosphere. High-resolution X-ray diffraction (XRD) patterns were collected using an X'Pert PRO Multi Purpose X-ray diffractometer (PANalytical, Almelo, The Netherlands) with a Cu Kα source operating at 40 kV and 30 mA. The TFT characteristics, including the transfer and output curves, were obtained using an HP4145B semiconductor analyzer. The temperature-dependent I−V measurements were obtained in the vacuum chamber of a probe station (Model M5VC) by using an HP4145B semiconductor parameter analyzer.

RESULTS AND DISCUSSION

Surface Modification of NCs. As-synthesized oleic acid-capped In_2O_3 NCs (In_2O_3 NC-OA) were synthesized by following the procedure we had previously published.[11] The as-synthesized In_2O_3 NC-OA was treated additionally to induce a ligand exchange to 2AP, 4ABA, and BA in the presence of HNO_3, yielding 2-aminopyridine-capped In_2O_3 NCs (In_2O_3 NC-2AP), 4-aminobenzoic-capped In_2O_3 NCs (In_2O_3 NC-4ABA), and benzoic acid-capped In_2O_3 NCs (In_2O_3 NC-BA). Furthermore, the addition of HNO_3, first, produced the salts of amino acids, including 2-ammonium nitrate pyridine (2AP·HNO_3) and 4-ammonium nitrate benzoic acid (4ABA·HNO_3), and, second, made these carboxylic acids more acidic by acting as a strong oxidizing agent. Therefore, the introduction of

DOI: 10.1021/acsami.5b02971
ACS Appl. Mater. Interfaces 2015, 7, 11660−11667

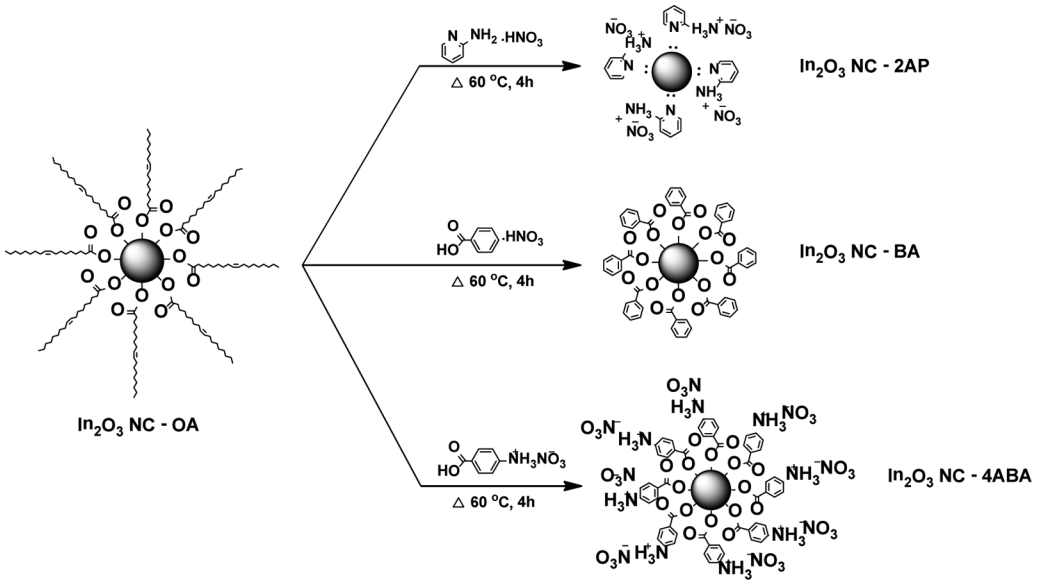

Figure 1. Schematic illustration of the ligand-exchange process with 2-aminopyridine (2AP), 4-aminobenzoic (4ABA), and benzoic acid (BA) in the presence of nitric acid.

HNO_3 into the ligand-exchange procedure affected both the ligand-exchange efficiency and the packing at the NCs surface, as schematically shown in Figure 1. These as-exchanged NCs can be readily re-dispersed in various polar, hydrophilic solvents, such as DMF, DMSO, and water, to form colloidal dispersions. In particular, the as-exchanged NC dispersions in DMF were the most stable without any detectable aggregation or precipitation. Figure 2 presents TEM images of the In_2O_3 NC samples used in this study, indicating that well-defined single-crystal In_2O_3 NCs were present before and after the ligand exchange. The size of the NCs was reduced due to surface etching (from 5.6 ± 0.4 nm for In_2O_3 NC-OA to 5.0 ± 0.4 nm for In_2O_3 NC-2AP, 5.3 ± 0.6 nm for In_2O_3 NC-BA, and 5.2 ± 0.6 nm for In_2O_3 NC-4ABA) during the ligand-exchange process in the presence of nitric acid (HNO_3). Structures were prevented from forming. The NCs did not aggregate after the surfaces had been modified. Subsequently, the XRD patterns (Figure 3a) confirm the high crystallinity of the In_2O_3 NC samples, showing that various diffraction peaks are assigned to the diffraction from the (211), (222), (400), (440), and (622) planes, respectively. Figure 3b shows the results of the TGA studies for In_2O_3 NC before and after the ligand exchange. The measurements were obtained by heating the samples from room temperature to 500 °C in ambient conditions. The total weight loss of the surface-modified as-exchanged NCs was of only 10% for the 2AP-capped NCs and BA-capped NCs, and 7% for the 4ABA-capped NCs, which is much lower than that of the as-synthesized NCs (~15%), providing further evidence of the complete exchange of OA ligands. The decomposition of these ligands was observed to be complete at 350 °C for OA, 310 °C for 2AP, 400 °C for BA, and 350 °C for 4ABA, and after that, no more decomposition was observed. Thus, curing temperatures of 150, 250, and 350 °C were selected for the NC TFTs in order to investigate the effects of the ligands on the properties of the NC TFTs. The hydrophilic nature and the reduced interparticle spacing of the surface-modified NCs suggest the removal of the original organic ligands, which is further confirmed via FTIR spectroscopy. The FT-IR of In_2O_3 NCs (Figure 3c) shows that the intensity of the aliphatic C−H stretching vibration at 2800−3000 cm^{-1} ascribed to the OA molecule significantly decreased after the surface had been modified. Additionally, after the ligand exchange, as salts of the amino acid NH_3^+ NO_3^- group formed in 2AP and 4ABA ligands, the broad NH_3^+ stretching band in the region 2600−3100 cm^{-1} was weak and impossible to distinguish. Furthermore, we assert that the vibration peak related to the COO- group and NO_3 groups were assigned to 1430−1650 cm^{-1}, and the previous 1297 cm^{-1} peak was a result of the C−N stretching vibration. Figure 3d shows a peak at 3005 cm^{-1} that corresponds to the =C−H stretching vibration on the OA ligand. After the ligand-exchange process, the =C−H peak disappeared, implying that the OA ligand had been entirely replaced by the new 2AP, BA, and 4ABA ligands.[16]

High-Performance Thin-Film NC Transistors. We demonstrate the utility of using solution-exchanged In_2O_3 NC-2AP, In_2O_3 NC-BA, and In_2O_3 NC-4ABA to spin-coat NC dispersions from DMF (~3 wt %) to fabricate the semiconducting channels of thin-film FETs. Figure 4 shows the device characteristics of the TFTs made from our as-exchanged NCs as well as SEM images of the TFT channels assembled from In_2O_3 NCs. Briefly, 3 wt % as-exchange In_2O_3 NCs in DMF were coated on thermally grown 100 nm thick SiO_2/p^{+2}-Si substrates via spin-coating, and the resulting NC thin films were heated to 350 °C for 3 h in an air atmosphere. Finally, the NC TFTs were completed by using a thermal evaporator at a pressure of 10^{-6} Torr with a shadow mask to deposit an aluminum source and drain electrodes with dimensions of 1000 μm (W) × 100 μm (L) . Parts b, c, f, g, k, and l of Figure 4 depict the representative drain current (I_{DS}) versus gate voltage (V_G) transfer curves that were obtained by sweeping V_G from −40 to +40 V at V_{DS} = 40 V and I_{DS} versus source drain voltage (V_{DS}) output curve as a function of the applied gate voltage, indicating that the as-exchanged In_2O_3 NC thin films formed n-channel FETs. The devices operate in an accumulation mode by applying a positive gate bias since the concentration of the majority carrier electrons contribute to the increase in I_{DS}. The device operation is adequately modeled by using the standard FET equation, $I_{DS} = (C_i\mu \times W/2L)(V_G - V_T)^2$, which

DOI: 10.1021/acsami.5b02971
ACS Appl. Mater. Interfaces 2015, 7, 11660−11667

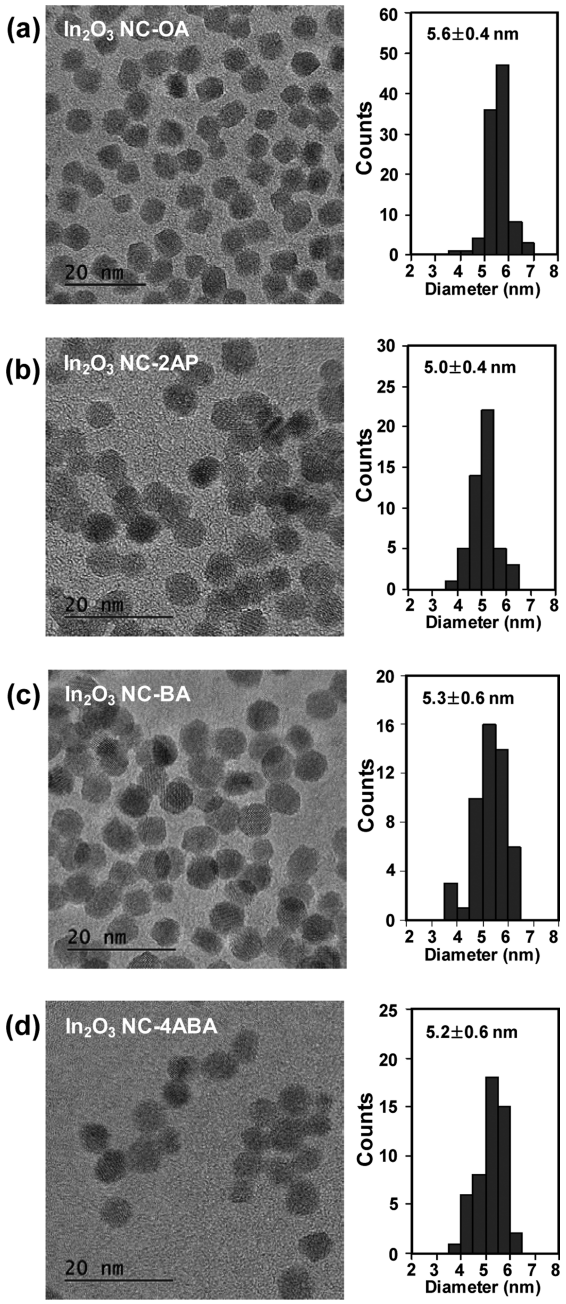

Figure 2. TEM images and sizing histogram of (a) as-synthesized In_2O_3 NC-OA, (b) as-exchanged In_2O_3 NC-2AP, (c) as-exchanged In_2O_3 NC-BA, and (d) as-exchanged In_2O_3 NC-4ABA.

employed the I_{DS} and $I_{DS}^{1/2}$ vs V_G data in Figure 4b,f,k to calculate the field-effect mobility for the electrons (μ), current modulation (I_{on}/I_{off}), threshold voltage (V_T), and subthreshold swing (SS). The summary in Table 1 shows the as-synthesized In_2O_3 NC capped with oleic acid produced TFTs that were highly insulating (μ = 0.43 ± 0.03 $cm^2/(V{\cdot}s)$).[11] The replacement of the bulky oleic acid with smaller 2AP molecule, BA molecule, and 4ABA molecule reduces the interparticle spacing from ~1.2 to ~0.4 nm and increases the In_2O_3 NC film mobility by a factor of 20. Remarkably, the TFT In_2O_3 NC-2AP channel shows the excellent mobility achieved to date of 9.5 $cm^2/(V{\cdot}s)$; I_{on}/I_{off} is above 10^7, with a threshold voltage of −12 V; the subthreshold swing, which is a critical metric for how well the device turns on and off, is of 2.3 V/decade, which is comparable to the as-synthesized In_2O_3 NC-OA. We can use the Einstein−Smoluchowski equation[18−20] to express the tunneling rate, Γ, which is proportional to the mobility, as follows:

$$\Gamma = \exp[-2(2m^*\Delta E/\hbar^2)^{1/2}\Delta x] \quad (1)$$

where m^*, ΔE, and Δx are the effective mass of the electrons, the height of the tunneling barrier, and the interdot distance between the NCs, respectively. Figure 5a presents the average mobility in the linear regime for the TFT devices fabricated using our method with 2AP, BA, and 4ABA organic ligands. The data are linear on a semilog plot, with the highest mobility for the three annealing conditions at 150, 250, and 350 °C of 2.3 × 10^{-3}, 5 × 10^{-2}, and 9.5 $cm^2/(V{\cdot}s)$, respectively, with the shortest molecule (2AP, ~4 Å), and the lowest mobility of 2.1 × 10^{-5}, 1.1 × 10^{-4}, and 2.6 $cm^2/(V{\cdot}s)$, respectively, measured with the longest molecule (4ABA, ~7.3 Å). Equation 1 shows that the tunneling rate (Γ) increases as the barrier height (ΔE) and NC interdot distance (Δx) decrease. Figure 5b shows the molecular structures and the frontier orbitals of the four OA, 2AP, BA, and 4ABA ligands used in this study, which is optimized using the DFT at B3LYP level and 6-31+G(d,p) basis set in Gaussian03.[21] Obviously, the electronic structure of the oleic acid is different from that of the shorter 2AP, BA, and 4ABA molecules, and the decrease in the HOMO−LUMO gap from the OA molecule (6.7 eV) is considerable, for example, to 2AP (5.4 eV). However, the similar HOMO−LUMO gap for 2AP, BA (5.7 eV), and 4ABA (5.0 eV) provides evidence that the increase in the mobility is in fact set by the length of the surface ligand rather than the different hopping barrier height.[17]

Temperature Dependence of Electron Mobility for In_2O_3 NC TFTs. The temperature-dependent charge transport behavior of the In_2O_3 NC TFTs cured at 150 °C was investigated in a vacuum below 10^{-2} Torr. The samples cured at 150 °C are chosen because the FT-IR spectra (Supporting Information Figure S1) shows the surface structures of the NCs in the thin films according to the curing temperatures. The 2AP, BA, and 4ABA ligand molecules are sustained on the NC surfaces after being cured at 150 °C, as confirmed by the appearance of peaks from 1550 to 1400 cm^{-1}. When the curing temperature increased to 250 °C, the exchange ligand on the In_2O_3 NC had mostly decomposed, which is consistent with the TG results shown in Figure 3b. Finally, when the NC thin films were cured at 350 °C, the IR peaks show that the organic functional groups had disappeared. For the SiO_2 gate electric layer, we observe a variation in the transfer curves of In_2O_3 NC TFT as the temperature increases from 173 to ~300 K. The results show that as the temperature increases, I_{DS} increases as well and V_T drifts toward the negative direction (Supporting Information Figure S2). A positive temperature coefficient is noted for the mobility ($d\mu/dT > 0$; Figure 6a), demonstrating a hopping transport mechanism instead of a band-like transport.[22−24] In the TFT devices, electron transport can take place near the interface between the NC films and the SiO_2, and additional trapping can occur at this interface that contains a large density of trapping sites associated with the surface hydroxyl groups.[25] A negative shift in V_T with an increase in temperature is explained by the generation of thermally activated carriers from traps within the band gap of the channel. Miller Abrahams provided the basis to calculate the mobility of the charge carrier in disordered colloidal NC solids at any temperature,[17,20,26] which is a product of the exponential distance and energy terms for which charge transport in NC

DOI: 10.1021/acsami.5b02971
ACS Appl. Mater. Interfaces 2015, 7, 11660−11667

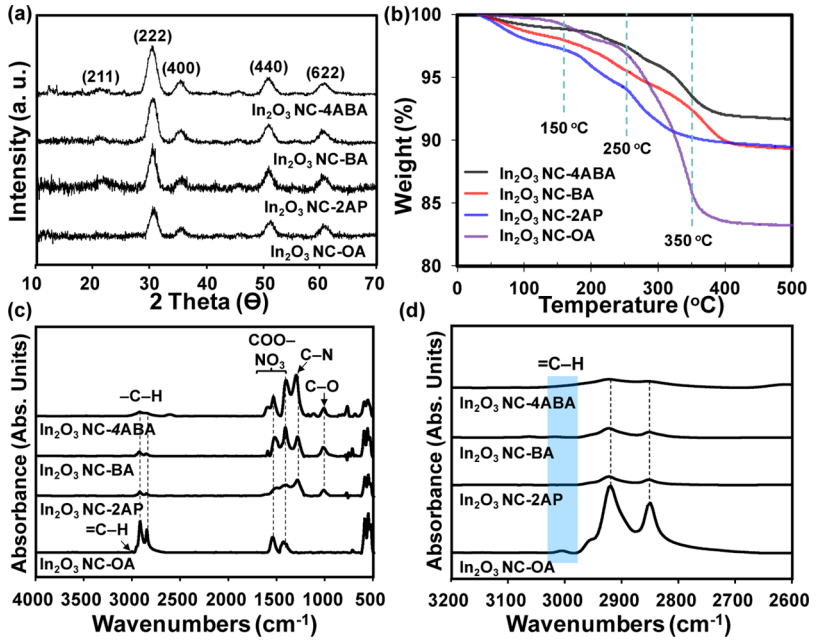

Figure 3. (a) XRD patterns, (b) TG curves, (c) FT-IR spectra, and (d) FT-IR spectra of C═C bond peaks of the as-synthesized In_2O_3 NC-OA and as-exchanged NC-2AP, NC-BA, and NC-4ABA.

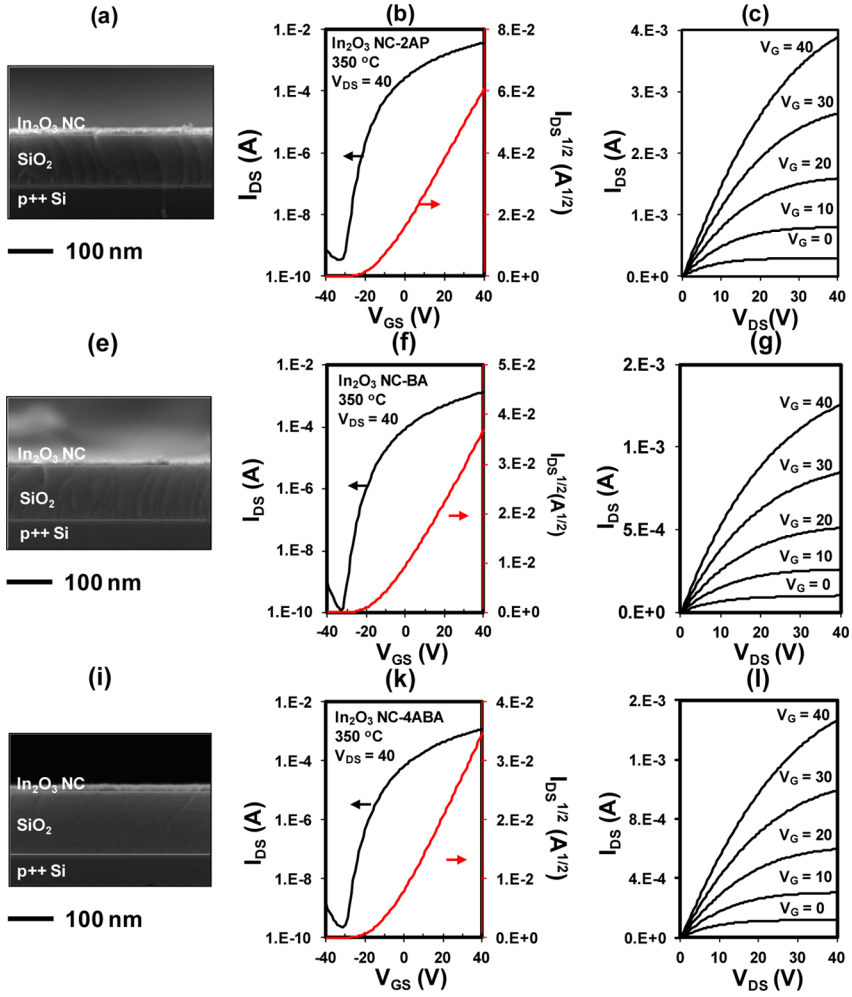

Figure 4. SEM of the cross-section of the devices used in this work (a, e, and i); transfer (b, f, and k) and output (c, g, and l) characteristics of In_2O_3 NC-2AP, In_2O_3 NC-BA, and In_2O_3 NC-4ABA TFTs annealed at 350 °C.

DOI: 10.1021/acsami.5b02971
ACS Appl. Mater. Interfaces 2015, 7, 11660−11667

Table 1. Performance Characteristics of the Tfts Made of an n-Channel In_2O_3 NCs Layer

In_2O_3 NC	curing temp (°C)	μ ($cm^2/(V{\cdot}s)$)	$I_{on/off}$	V_T (V)	SS (V/decade)
OA[a]	350	0.4 ± 0.03	$(8.3 \pm 1.0) \times 10^2$	−17.9 ± 4.8	8.5 ± 2.0
2AP	150	$(2.3 \pm 0.1) \times 10^{-3}$	$(2.4 \pm 1.0) \times 10^4$	−14.7 ± 2.5	4.3 ± 2.1
2AP	250	$(4.7 \pm 0.5) \times 10^{-2}$	$(5.2 \pm 2.0) \times 10^4$	−20.1 ± 2.5	5.4 ± 2.5
2AP	350	9.5 ± 0.2	$(1.7 \pm 1.0) \times 10^7$	−13.4 ± 2.1	2.3 ± 0.2
BA	150	$(3.6 \pm 0.5) \times 10^{-4}$	$(9.0 \pm 1.0) \times 10^3$	2.0 ± 5.0	1.9 ± 0.5
BA	250	$(8.8 \pm 1.5) \times 10^{-3}$	$(2.6 \pm 4.0) \times 10^4$	−3.7 ± 2.0	2.4 ± 2.0
BA	350	3.07 ± 1.1	$(1.2 \pm 2.0) \times 10^7$	−10.5 ± 4.8	2.5 ± 1.1
4ABA	150	$(2.3 \pm 0.5) \times 10^{-5}$	$(4.6 \pm 2.5) \times 10^2$	4.1 ± 2.8	1.3 ± 1.2
4ABA	250	$(1.2 \pm 1.5) \times 10^{-4}$	$(1.2 \pm 2.0) \times 10^3$	2.7 ± 0.8	2.5 ± 0.9
4ABA	350	2.6 ± 0.2	$(5.3 \pm 1.0) \times 10^6$	−10.2 ± 4.7	2.5 ± 0.5

[a]Data for In_2O_3 NCs capped with oleic acid (OA), as-synthesized, are extracted from ref 11. Mobility calculated from the equation $\mu = (2I_{DS}L)/[WC_i(V_G - V_{th})^2]$.

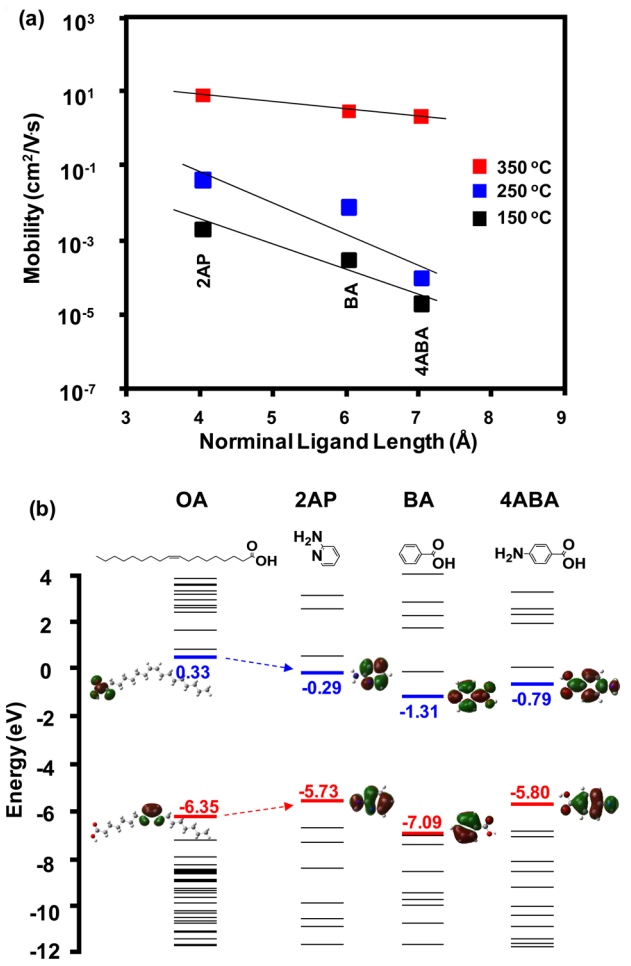

Figure 5. (a) Electron mobility as a function of the ligand length in In_2O_3 NC TFTs. (b) Molecular structures and frontier orbitals of oleic acid (OA), 2-aminopyridine (2AP), benzoic acid (BA), and 4-aminobenzoic acid (4ABA) ligands optimized using density functional theory (DFT) at the B3LYP level and 6-31+G(d,p) basis set in Gaussian03, respectively. The highest occupied molecular orbital (HOMO) and lowest unoccupied molecular orbital (LUMO) are indicated with red and blue colors, respectively.

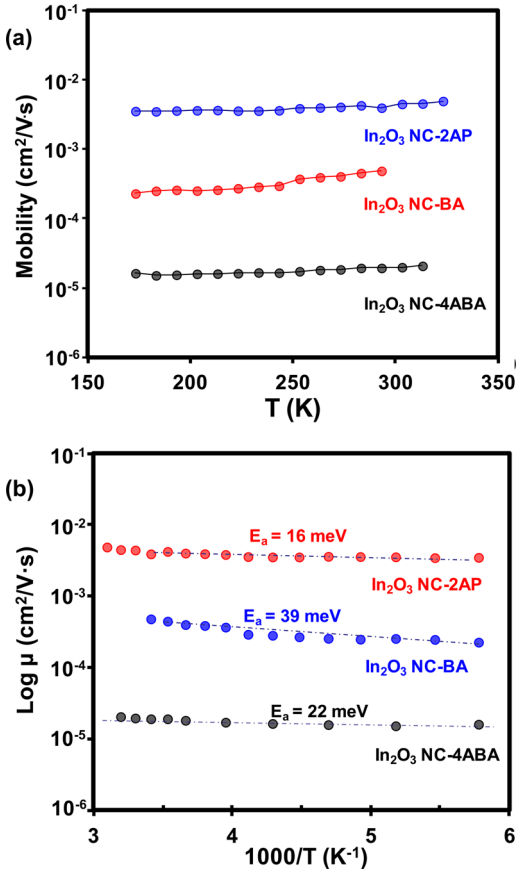

Figure 6. (a) Temperature dependence of the electron mobility and (b) Arrhenius plot of μ versus $1000/T$ in vacuum for In_2O_3 NC TFTs, film cured at 150 °C: blue line, In_2O_3 NC-2AP; red line, In_2O_3 NC-BA; black line, In_2O_3 NC-4ABA.

solids occurs by a nearest-neighbor-hopping (NNH)-activated process, and a series of incoherent tunneling transitions take place between adjacent NCs. The relation $\sigma = en\mu$,[27−31] indicates that the activation energy of such a thermally activated process is described by the following equation

$$\mu = \mu_0 \exp(-E_a/k_B T) \quad (2)$$

Furthermore, the activation energy (E_a) can be derived according to the Arrhenius plot for μ. As shown in Figure 6b, the $\log(\mu)-1000/T$ plots exhibited a good linear dependency, indicating that the thermally activated carrier transport process was governed by a consistent energy barrier. The activation energy for crystalline indium oxide ranges from 16 meV for In_2O_3 NC-2AP to 39 meV for In_2O_3 NC-BA and 22 meV for In_2O_3 NC-4ABA. This difference in the values of the activation energy can be explained by the difference in the free carrier concentration, which is a result of trapping at the boundary of

DOI: 10.1021/acsami.5b02971
ACS Appl. Mater. Interfaces 2015, 7, 11660−11667

NC. The decrease in the free carrier concentration leads to a displacement in the Fermi level to the bulk of the band gap and, accordingly, to an increase in the activation energy.

CONCLUSION

The principal findings of this study are summarized as follows. The temperature-dependent and surface ligand length-dependent electron transport in In_2O_3 NC films was thoroughly investigated. (i) We demonstrated that various short organic ligands can bind to the surface of In_2O_3 NCs to provide colloidal stability for the NC dispersions in DMF. These new ligands represent a useful class of short, abundant, nontoxic, compact ligands for use in a solution ligand-exchange process. The shorter interparticle distance greatly facilitates electronic coupling between adjacent NCs, leading to a high electron mobility. For instance, 2-aminopyridine-capped NC arrays exhibited a high field-effect electron mobility of ~9.5 $cm^2/(V \cdot s)$, which is comparable to the record mobility for solution-processed In_2O_3 NC arrays. (ii) The electron mobility increases exponentially with a decrease in the ligand length. (iii) At a low temperature from 173 to ~300 K, electron transport followed the nearest-neighbor hopping. We believe that this study provides a fundamental understanding of the charge transport in NC films, and this will promote the further development of In_2O_3 NCs into thin-film transistors.

ASSOCIATED CONTENT

Supporting Information

Figures showing FT-IR spectra of the In_2O_3 NC-OA, In_2O_3 NC-2AP, In_2O_3 NC-B, and In_2O_3 NC-4ABA thin films cured at 150, 300, and 350 °C (Figure S1) and $I_{DS}-V_{GS}$ characteristic of TFT based on In_2O_3 NCs (film cured at 150 °C) measured at low temperature from 173 to 323 K (Figure S2). The Supporting Information is available free of charge on the ACS Publications website at DOI: 10.1021/acsami.5b02971.

AUTHOR INFORMATION

Corresponding Author

*E-mail: hdjeong@chonnam.ac.kr.

Notes

The authors declare no competing financial interest.

ACKNOWLEDGMENTS

This work was supported by the Material Original Technology Program (10041222), funded by the Ministry of Knowledge Economy (MKE, Korea).

REFERENCES

(1) Facchetti, A.; Marks, T. J. *Transparent Electronics: From Synthesis to Applications*; John Wiley & Sons: Chichester, U.K., 2010.

(2) Nakazawa, H.; Ito, Y.; Matsumoto, E.; Adachi, K.; Aoki, N.; Ochiai, Y. The Electronic Properties of Amorphous and Crystallized In_2O_3 Films. *J. Appl. Phys.* **2006**, *100*, 093706-1−093706-8.

(3) Gupta, A.; Cao, H.; Parekh; Rao, K. K. V.; Raju, A. R.; Waghmare, U. Room Temperature Ferromagnetism in Transition Metal (V, Cr, Ti) Doped In_2O_3. *J. Appl. Phys.* **2007**, *101*, 09N513-1−09N513-3.

(4) Kim, H. S.; Byrne, P. D.; Facchetti, A.; Mark, T. J. High Performance Solution-Processed Indium Oxide Thin-Film Transistors. *J. Am. Chem. Soc.* **2008**, *130* (38), 12580−12581.

(5) Kim, M.-G.; Kantzidis, M. G.; Facchetti, A.; Mark, T. J. Low-Temperature Fabrication of High-Performance Metal Oxide Thin-Film Electronics via Combustion Processing. *Nat. Mater.* **2011**, *10*, 382−388.

(6) Hwang, Y.-H.; Jeon, J.-H.; Bae, B.-S. Post-Humid Annealing of Low-Temperature Solution-Processed Indium Based Metal Oxide TFTs. *Electrochem. Solid-State Lett.* **2011**, *14* (7), H303−H305.

(7) Hwang, Y.-H.; Seo, J.-S.; Yun, J. M.; Park, H.-J.; Yang, S.-Y.; Park, S.-H.; Bae, B.-S. An 'aqueous route' for The Fabrication of Low-Temperature-Processable Oxide Flexible Transparent Thin-Film Transistors on Plastic Substrates. *NPG Asia Mater.* **2013**, *5*, No. e45.

(8) Seo, W.-S.; Jo, H.-H.; Lee, K.; Park, J. T. Preparation and Optical Properties of Highly Crystalline, Colloidal, and Size-Controlled Indium Oxide Nanoparticles. *Adv. Mater.* **2003**, *15* (10), 795−797.

(9) Liu, Q.; Lu, W.; Ma, A.; Tang, J.; Lin, J.; Fang, J. Study of Quasi-Monodisperse In_2O_3 Nanocrystals: Synthesis and Optical Determination. *J. Am. Chem. Soc.* **2005**, *127*, 5276−5277.

(10) Ye, E.; Zhang, S.-Y.; Lim, H. S.; Liu, S.; Han, M.-Y. Morphological Tuning, Self-Assembly and Optical Properties of Indium Oxide Nanocrystals. *Phys. Chem. Chem. Phys.* **2010**, *12*, 11923−11929.

(11) Pham, H. T.; Jeong, H.-D. Non-monotonic Size Dependence of Electron Mobility in Indium Oxide Nanocrystals ThinFilm Transistor. *Bull. Korean Chem. Soc.* **2014**, *35*, 2505−2511.

(12) Kuno, M.; Lee, J. K.; Dabbousi, B. O.; Mikulec, F. V.; Bawendi, M. G. The Band Edge Luminescence of Surface Modified CdSe Nanocrystallites: Probing The Luminescing State. *J. Chem. Phys.* **1997**, *106*, 9869−9882.

(13) Ridley, B. A.; Nivi, B.; Jacobson, J. M. All-Inorganic Field Effect Transistors Fabricated by Printing. *Science* **1999**, *286*, 746−749.

(14) Brown, P. R.; Kim, D.; Lunt, R. R.; Zhao, N.; Bawendi, M. G.; Grossman, J. C.; Bulovic, V. Energy Level Modification in Lead Sulfide Quantum Dot Thin Films through Ligand Exchange. *ACS Nano* **2014**, *8* (6), 5863−5872.

(15) Voznyy, O.; Zhitomirsky, D.; Stadler, P.; Ning, Z.; Hoogland, S.; Sargent, E. H. A Charge-Orbital Balance Picture of Doping in Colloidal Quantum Dot Solids. *ACS Nano* **2012**, *6* (9), 8448−8455.

(16) Dao, D. T.; Hafer, M. E.; Beloborodov, I. S.; Jeong, H.-D. Thioacetic-Acid Capped PbS Quantum Dot Solids Exhibiting Thermally Activated Charge Hopping Transport. *Bull. Korean Chem. Soc.* **2014**, *35*, 457−465.

(17) Liu, Y.; Gibbs, M.; Puthussery, J.; Gaik, S.; Ihly, R.; Hillhouse, H. W.; Law, M. Dependence of Carrier Mobility on Nanocrystal Size and Ligand Length in PbSe Nanocrystal Solids. *Nano Lett.* **2010**, *10*, 1960−1969.

(18) Talapin, D. V.; Lee, J.-S.; Kovalenko, M. V.; Shevchenko, E. V. Prospects of Colloidal Nanocrystals for Electronic and Optoelectronic Applications. *Chem. Rev.* **2010**, *110*, 389−458.

(19) Vanmaekelbergh, D.; Liljeroth, P. Electron-Conducting Quantum Dot Solids: Novel Materials Based on Colloidal Semiconductor Nanocrystals. *Chem. Soc. Rev.* **2005**, *34*, 299−312.

(20) Pham, H. T.; Jeong, H.-D. Solution-Processed Inorganic Thin Film Transistors Fabricated from Butylamine-Capped Indium-Doped Zinc Oxide Nanocrystals. *Bull. Korean Chem. Soc.* **2014**, *35*, 494−500.

(21) Frisch, M. J.; Trucks, G. W.; Schlegel, H. B.; Scuseria, G. E.; Robb, M. A.; Cheeseman, J. R.; Montgomery, J. A., Jr.; Vreven, T.; Kudin, K. N.; Burant, J. C.; Millam, J. M.; Lyengar, S. S.; Tomasi, J.; Barone, V.; Mennucci, B.; Cossi, M.; Scalmani, G.; Rega, N.; Petersson, G. A.; Nakatsuji, H.; Hada, M.; Ehara, M.; Toyota, K.; Fukuda, R.; Hasegawa, J.; Ishida, M.; Nakajima, T.; Honda, Y.; Kitao, O.; Nakai, H.; Klene, M.; Li, X.; Knox, J. E.; Hratchian, H. P.; Cross, J. B.; Adamo, C.; Jaramillo, J.; Gomperts, R.; Stratmann, R. E.; Yazyev, O.; Austin, A. J.; Camml, R.; Pomelli, C.; Ochterski, J. W.; Ayala, P. Y.; Morokuma, K.; Voth, G. A.; Salvador, P.; Dannenberg, J. J.; Zakrzewski, V. G.; Dapprich, S.; Daniels, A. D.; Strain, M. C.; Farkas, O.; Malick, D. K.; Rabuck, A. D.; Raghavachari, K.; Foresman, J. B.; Ortiz, J. V.; Cui, Q.; Baboul, A. G.; Clifford, S.; Cioslowski, J.; Stefanov, B. B.; Liu, G.; Liashenko, A.; Piskorz, P.; Komaromi, I.; Martin, R. L.; Fox, D. J.; Keith, T.; Al-Laham, M. A.; Peng, C. Y.; Nanayakkara, A.; Challacombe, M.; Gill, P. M. W.; Johnson, B.; Chen, W.; Wong, M. W.; Gonzalez, C.; Pople, J. A. *Gaussian03*, RevisionD.1; Gaussian: Wallingford, CT, USA, 2005.

DOI: 10.1021/acsami.5b02971
ACS Appl. Mater. Interfaces 2015, 7, 11660−11667

(22) Sakanoue, T.; Sirringhaus, H. Band-like Temperature Dependence of Mobility in a Solution-Processed Organic Semiconductor. *Nat. Mater.* **2010**, *9*, 736−740.
(23) Nelson, S. F.; Lin, Y.-Y.; Gundlach, D. J.; Jackson, T. N. Temperature-Independent Transport in High-Mobility Pentacene Transistors. *Appl. Phys. Lett.* **1998**, *72*, 1854−1856.
(24) Li, J.; Zhao, Y.; Tan, H.-S.; Guo, Y.; Di, C.-A.; Yu, G.; Liu, Y.; Lin, M.; Lim, S.-H.; Zhou, Y.; Su, H.; Ong, B. S. A Stable Solution-Processed Polymer Semiconductor with Record High-Mobility for Printed Transistors. *Sci. Rep.* **2012**, *2*, 754-1−754-9.
(25) Chua, L.-L.; Zaumseil, J.; Chang, J.-F.; Ou, E. C. W.; Ho, P. K. H.; Sirringhaus, H.; Friend, R. H. General Observation of N-Type Field-Effect Behaviour in Organic Semiconductors. *Nature* **2005**, *434*, 194−199.
(26) Miller, A.; Abrahams, E. Impurity Conduction at Low Concentrations. *Phys. Rev.* **1960**, *120*, No. 745.
(27) Philippe, G.-S. Electrical Transport in Colloidal Quantum Dot Films. *J. Phys. Chem. Lett.* **2012**, *3*, 1169−1175.
(28) Kang, M. S.; Sahu, A.; Norris, A. J.; Frisbie, C. D. Size- and Temperature-Dependent Charge Transport in PbSe Nanocrystal Thin Films. *Nano Lett.* **2011**, *11*, 3887−3892.
(29) Jang, J.-Y.; Liu, W.; Son, J.-S.; Talapin, D. V. Temperature-Dependent Hall and Field-Effect Mobility in Strongly Coupled All-Inorganic Nanocrystal Arrays. *Nano Lett.* **2014**, *14*, 653−662.
(30) Forsh, E. A.; Marikutsa, A. V.; Martyshov, M. N.; Forsh, P. A.; Rumyantseva, M. N.; Gas'kov, A. M.; Kashkarov, P. K. Charge Carrier Transport in Indium Oxide Nanocrystals. *J. Exp. Theor. Phys.* **2010**, *111* (4), 653−658.
(31) Huang, X.; Wu, C.; Lu, H.; Ren, F.; Chen, D.; Jiang, R.; Zhang, R.; Zheng, Y.; Xu, Q. Temperature and Gate Bias Dependence of Carrier Transport Mechanisms in Amorphous Indium-Gallium-Zinc Oxide Thin Film Transistor. *Solid-State Electron.* **2013**, *86*, 41−44.

DOI: 10.1021/acsami.5b02971
ACS Appl. Mater. Interfaces 2015, 7, 11660−11667